Instrumentation for the Assessment of Parafoil Performance

Greg Noetscher[1] and Justin Barber[2]
US Army Natick Soldier Center, Natick, MA, 01760

The Natick Soldier Center (NSC) in conjunction with the Joint Precision Airdrop System (JPADS) Advanced Concept Technology Demonstration (ACTD) Program has developed a suite of affordable instrumentation packages to support the testing and evaluation of prototype decelerator systems. The units can be mounted on the payload or on an Airborne Guidance Unit (AGU). In addition to being utilized for the collection of flight dynamics data of steer-able gliding systems, such as parafoils, the same packages may also be used under a ballistic parachute for the purpose of measuring the wind profile over the dropzone. This paper details the design methodology of the instrumentation packages and presents representative data collected during their use in flight test.

I. Introduction

Over the past two years the US Army Natick Soldier Center (Natick) has pursued the advancement of a core competency in the development of instrumentation suitable to characterize the flight dynamics of parachute systems being tested by the organization in support of its airdrop system development programs. In particular, the high performance gliding systems being developed under the JPADS ACTD Program have instrumentation and data collection requirements beyond those for conventional ballistic systems. During the ongoing JPADS test programs, the instrumentation developed by Natick and discussed in this paper has been demonstrated as highly reliable, robust, and effective. No flight data has been lost due to failure of the instrumentation packages to record. Further, data collected by the instrumentation has proven critical in making sound program-level technical decisions.

II. Hardware

The following section outlines general information regarding the hardware used in the data acquisition system.

1) Data Logger

The heart of the data acquisition system is an integrated, 32-bit microcontroller that blends power management and data manipulation attributes with peripheral subsystems. The central processing unit is connected to the queued serial module (QSM) via a common intermodule bus (IMB). The basic power consumption of the microcontroller is kept low due to its high-density complementary metal-oxide semiconductor (HCMOS) architecture. The power can be further reduced by judiciously controlling the system clock or completely minimized by running in special low-power modes.

The QSM consists of two separate interfaces: the queued serial peripheral interface (QSPI), and the serial communication interface (SCI). The QSPI offers expansion to peripheral devices through a full-duplex, synchronous bus. This interface can be expanded to include up to 16 different devices. The SCI provides either full- or half-duplex communication capabilities and includes dual data buffers. A wide range of baud rates is supported and can be modified via software.

Analog data is sampled via an 8-channel, 16-bit analog-to-digital converter (ADC) that contains a synchronous serial interface. Typical power consumption is on the order of 10mW but can be as low as 15uW in shutdown mode. The chip also includes an on-board multiplexer and can support samples rates up to 100kHz.

All data sampled by the system can be accessed via a compact flash card or downloaded over Universal Serial Bus (USB). This methodology facilitates very fast download times resulting in faster data availability for analysis.

---

[1] Electrical Engineer, JPADS ACTD
[2] Aerospace Engineer, JPADS ACTD

This material is declared a work of the U.S. Government and is not subject to copyright protection in the United States.

2) Inertial Sensor Module

Inertial data is provided by a tri-axial, six degree-of-freedom integrated sensor. MEMS accelerometers and rate gyroscopes are mounted orthogonally to produce continuous analog data. This solid-state construction has no moving parts, can operate at low power, is reliable, and has a low sensitivity to various environmental factors like shock and vibration. A variety of acceleration and angular rate ranges are supported and the selection of the proper sensors depends on the application. In general, acceleration data has a bandwidth of DC to 150Hz while the angular rate bandwidth is DC to 25Hz.

This integrated sensor is housed in a die-cast anodized aluminum enclosure and is rated to survive a max G load of 1000G while power is applied. Its tri-axial current draw is nominally 50mA.

3) GPS

The Global Positioning System (GPS) unit offers a reliable source of position, velocity, and time (PVT) data. The unit supports all-in-view satellite tracking with a 12-channel correlator. Improved accuracy, integrity, and availability of GPS can be obtained when operating in Satellite Based Augmentation System mode (SBAS). This GPS device is equipped for SBAS by using the Wide Area Augmentation System (WAAS). PVT data can be output at up to 5Hz. To supplement the software abilities of the unit, an active antenna is used to boost the received signal. The antenna provides 12dB of amplification.

4) Enclosure

In order to house the aforementioned electronics, a custom enclosure was designed and built. The instrumentation box is constructed of 6061 aluminum in order to withstand the rigorous airdrop environment. Apart from it's primary protection purpose, the package provides a solid base for mounting accelerometers. Data acquisition can be triggered by lanyard pull locally or via a remote switch that allows access to various data logger functions from hard to reach places. In this way, the system can be buried in the unit being tested and not be disturbed throughout a testing session. An example of the enclosure mounted on a test article is shown in Figure 1.

Figure 1. Mounting of Data Package and Switch on CDS Bundle.

III. Analog Data Processing

1) Data Sampling

Data is acquired at two different sample rates, f_s, based on time. For the first 30 seconds of measurement, the sample rate is fixed at 1000Hz. After 30 seconds, the rate changes to 200Hz. This data acquisition strategy can be modified via software and was chosen to fit the airdrop application. The most dynamic portion of decelerator flight takes place on exit of the aircraft. Therefore, a high sample rate is desired to fully capture all events.

In order to process the analog signals of the inertial sensor, there must be an analog-to-digital (A/D) conversion performed by the ADC described above. The result is a discrete time, discrete amplitude signal accomplished by two separate processes: sampling and quantization. Sampling a continuous time signal produces a discrete time

signal where the time between samples is $1/f_s$. Quantization converts a discrete time, continuous amplitude signal into a discrete time, discrete amplitude signal. In this way, the original analog signal that can take on an infinite number of values is represented by a finite set of values. Any difference between the original input and quantized output is called quantization error.

When attempting to fully reconstruct the original analog signal, the sampling frequency must be sufficiently high enough to avoid aliasing. The absence of aliasing implies that all frequency components of a signal are represented distinctly. The sampling theorem states that a signal can be perfectly replicated if it is sampled at a rate higher than twice the highest frequency in the signal. This sampling rate is commonly referred to the Nyquist rate. By following the sampling theorem, aliasing can be prevented.

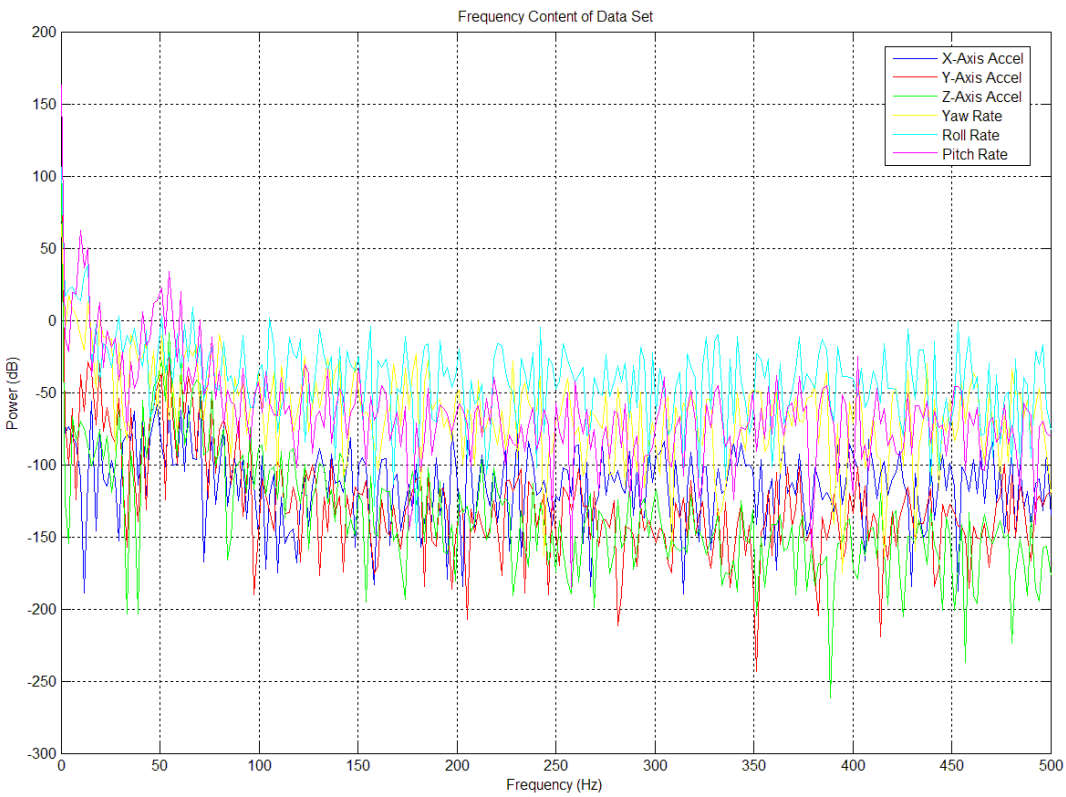

Figure 2. Frequency Content of Sample Data Set.

A frequency analysis of the system must be performed to determine the highest frequency in the system. One method of analysis is to take the Fourier transform of the signal and calculate the power spectral density. When graphed, the power spectrum provides a visual tool that maps a signal's power to a particular frequency.

Figure 2 displays the frequency content of an example set of data to include X-, Y-, and Z-accelerations and roll, pitch, and yaw rates. The exact frequency content varies from signal to signal, but it is clear to see that by around 100Hz, the power of each signal has declined significantly. By 200Hz, the data set is approaching –200dB. It is therefore safe to assume that sampling at 1000Hz will capture the entire desired signal.

2) Data Filter Selection and Application

There are a number of common filters that can be applied to dramatically clean up data and reduce the possibility of noise corruption in the system. The filter is chosen based on a desired magnitude and phase response in the frequency domain. In this application, a low-pass filter that passes all data below a specified frequency and attenuates data above the specified is needed. If a linear-phase requirement in the passband is desired, a finite

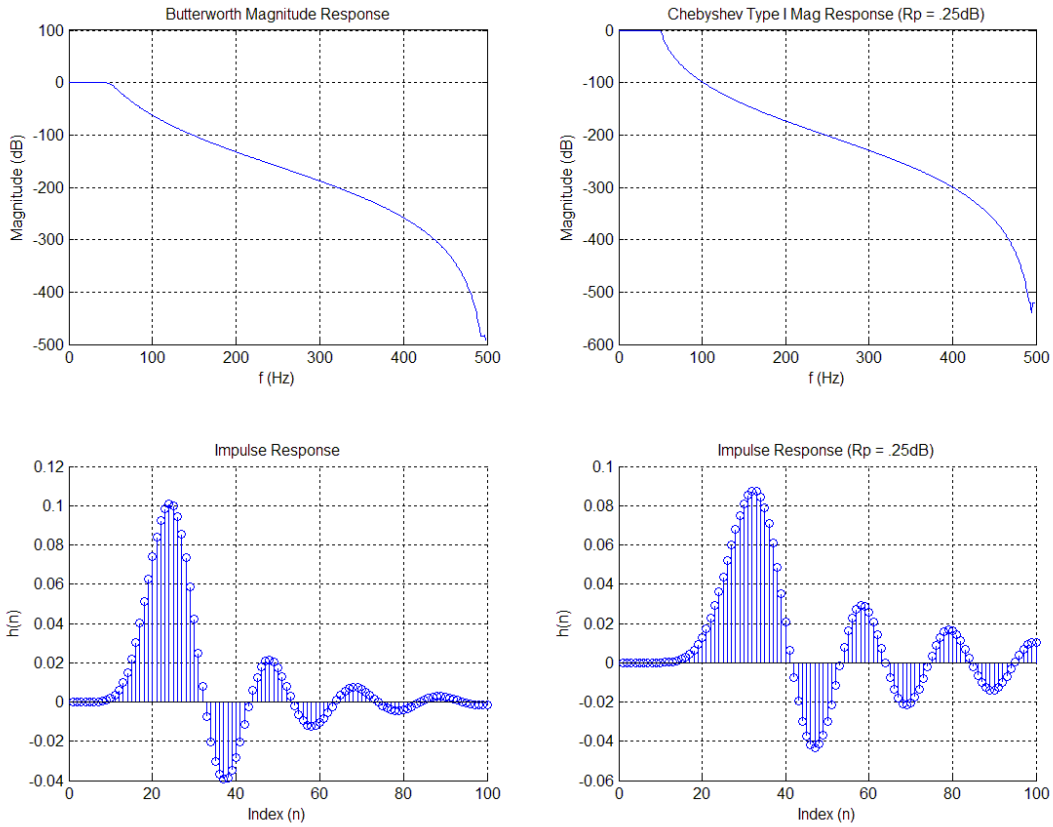

Figure 3. Magnitude and Impulse Responses for Butterworth and Chebyshev Type I Filters.

impulse response (FIR) filter should be used. In applications where linear-phase is not a requirement, infinite impulse response (IIR) filters are used because they generally have lower sidelobes in the stopband. Running the data through the filter produces phase distortion. Reversing the data, and then passing it through the filter again will negate the effects of phase distortion. Butterworth, Chebyshev Type I and Type II, and Elliptical filters are four of the most common IIR filters and will be compared below.

Figures 3 and 4 display the magnitude and impulse responses of 10th order Butterworth, Chebyshev Type I, Chebyshev Type II, and Eliptical filters. All filters have a –3dB frequency (low-pass cutoff frequency) of 50Hz. Ideally, the transition between the passband and the stopband would be instantaneous. In practice, the transition slope is dictated by the filter order. The higher the order, the steeper the slope, and therefore, the quicker the transition between passband and stopband.

The Butterworth filter is monotonic in both the passband and the stopband. There is no amplification in the passband and attenuation is severe in the stopband. Butterworth filters are all-pole filters.

The Chebyshev Type I filter differs in that it displays equiripple characterisitics in the passband. The gain of the signal will vary equally between two values. While the gain variation remains constant, the transition slope between the two values can differ. This filter is an all-pole filter that is monotonic in the stopband.

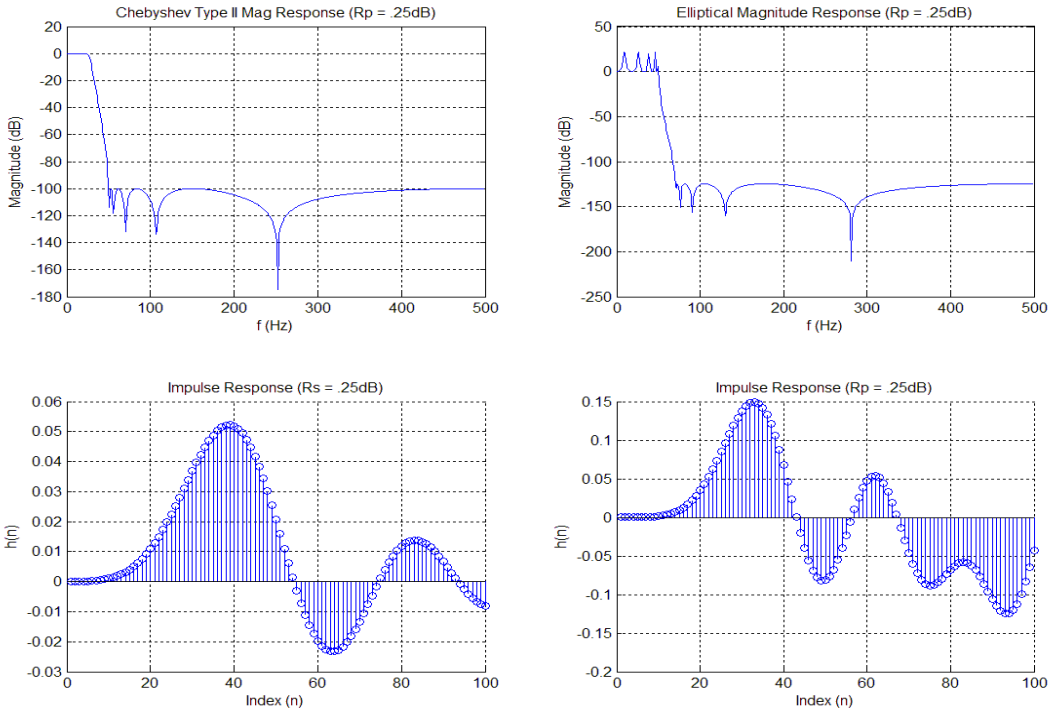

Figure 4. Magnitude and Impulse Responses for Chebyshev Type II and Eliptical Filters.

The Chebyshev Type II filter exhibits equiripple behavior in the stopband and is monotonic in the passband. The Type II family of filters contain both poles and zeros.

Elliptial filters have equiripple characteristics in both the passband and the stopband. Elliptical filters have the smallest transition bandwidth of the four filters discussed.

When applied to the data, these various filters produce some interesting results. In the following discussion, the filters have been applied to the x-axis acceleration data. As seen in Figure 2, the power of this particular signal concentrated primarily above 50Hz. Let us pass all information below 50Hz and attenuate all data thereafter.

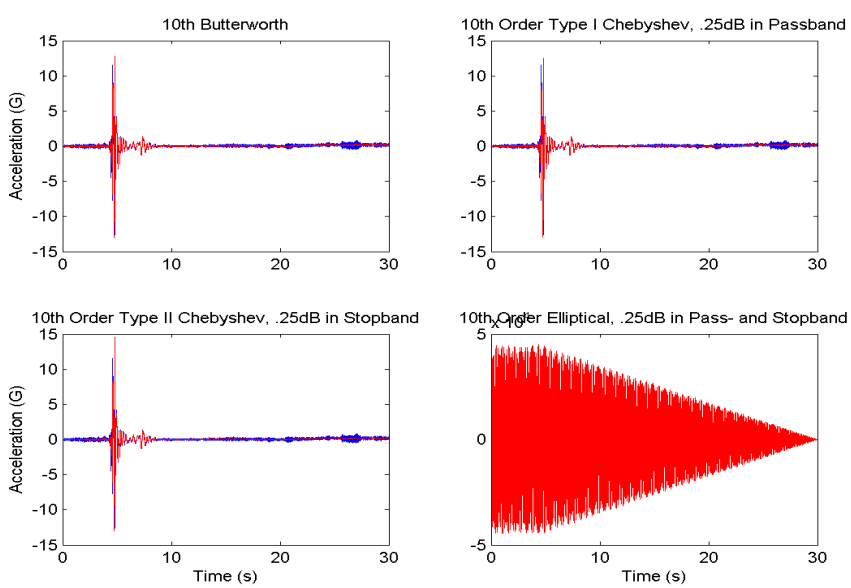

Figure 5. Original and Filtered Data.

The results of applying the four filters described above are shown in Figure 5 where original data is blue, and processed data is red. The elliptical filter has amplified both low and high frequency noise to the point of obscuring the original signal.

Figure 6 shows a closer look at the original and filtered signals. Notice that there is no instance of phase distortion. It is also interesting to note that the Butterworth and Chebyshev Type I filters follow the higher frequency movements slightly better than the Chebyshev Type II filter, though the higher frequencies are not amplified. Results that follow were obtained using a Butterworth filter.

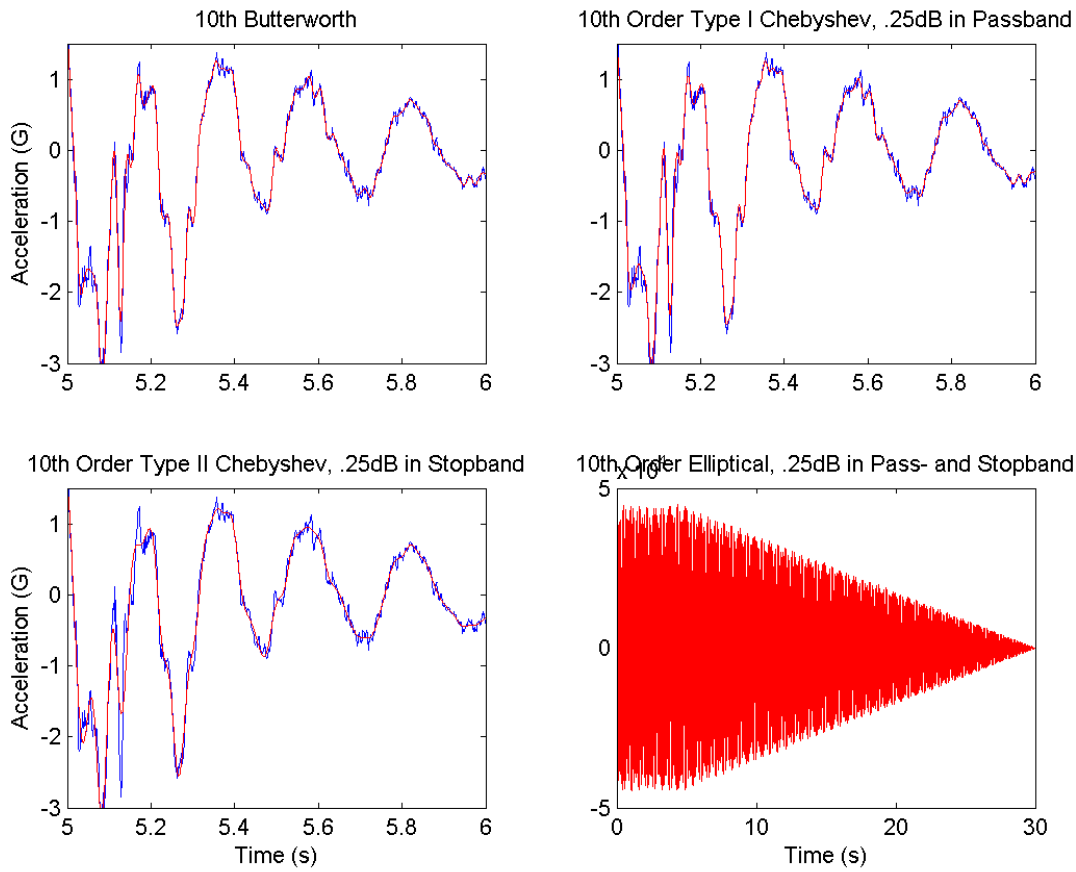

Figure 6. A Closer Look at Original and Filtered Data.

IV. Telemetry and Inertial Data

After applying a filter to minimize errors due to system noise, numerical methods of integration are applied to the data to recover a variety of information including yaw and pitch angles. Figure 7 displays the pitch angle of a CDS bundle released from a C-130. Notice that the bundle starts to slide off the airplane ramp and tips over at about 4 s. For the next 20s, the parafoil used to guide the system goes through a dynamic opening period . As the canopy becomes stable, the drastic movement of the payload begins to dampen out.

When instrumentation is placed on both the payload and inside the AGU, relationships between the two bodies can be observed. Figure 8 provides a fine example of this test strategy. The system under test is a 10,000lb capable 3,470 sq ft parafoil and AGU that was controlling 8,000lbs suspended by an Enhanced Container Delivery System (ECDS) platform. When in flight, there was concern that the motion of the payload could dictate the control of the system by the AGU. As seen in this figure, the AGU yaw angle oscillates at almost twice the frequency of the payload yaw angle. Since the AGU is suspended between the payload and the canopy, it is reacting to the payload movement. If the heading of the system were to be derived from a measurement on the AGU, the heading data

would be invalid if the AGU was dragged to an angle by the payload and any further guidance and control provided by the AGU could be erroneous.

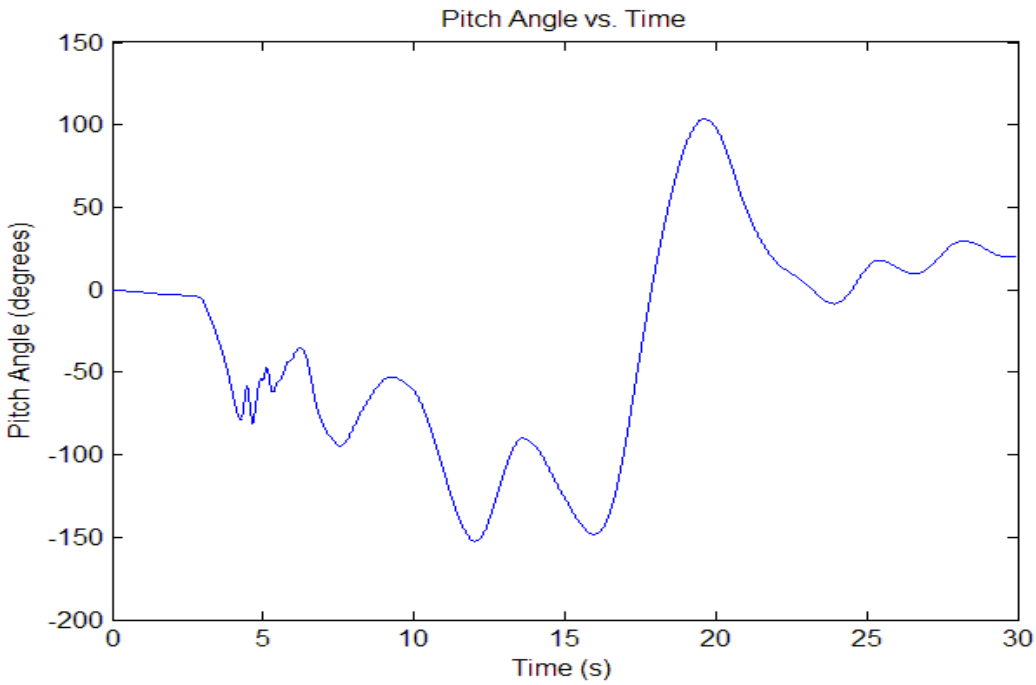

Figure 7. Pitch Angle Derived from Pitch Rate

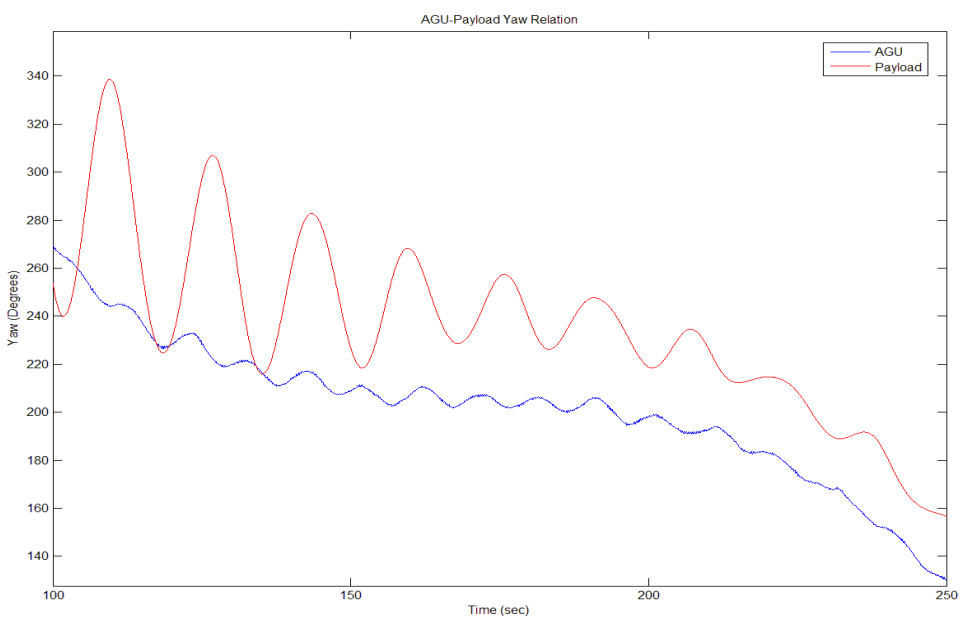

Figure 8. Payload and AGU Yaw Angles.

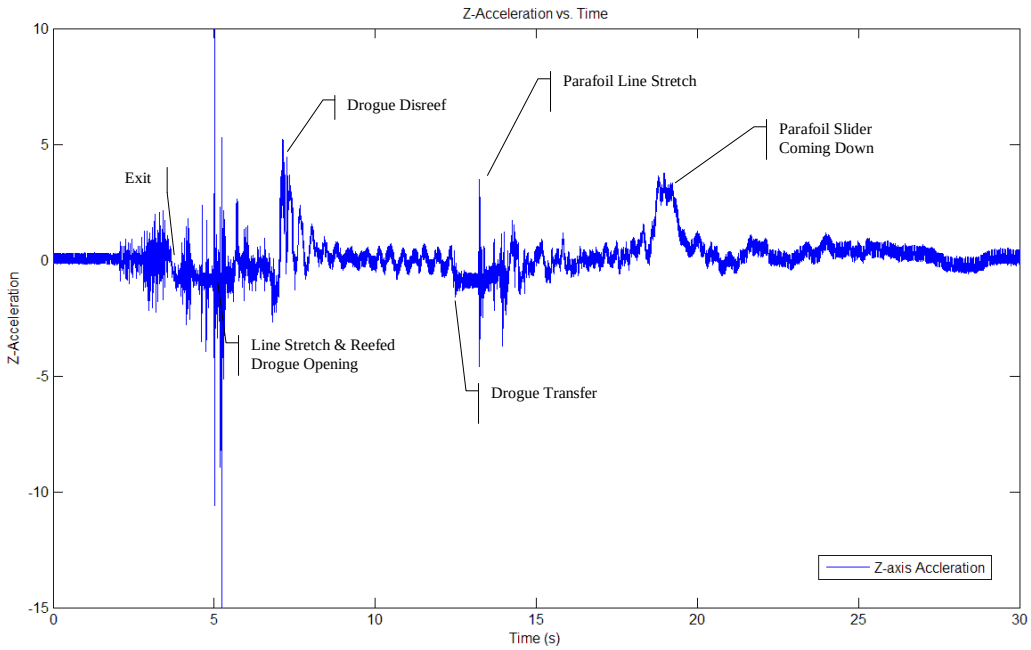

Figure 9. Z-Axis Acceleration Data.

As described above, the first 30s of a flight are sampled at 1000Hz. A number of dynamic events that occur during this time can be captured from post-flight analysis. Some of these events are summarized in Figure 9 including gravity-extracted exit from the aircraft, drogue inflation and transfer, and parafoil inflation.

Position data from both the payload and a ballistic parachute can provide significant insight into the system. Post-processing routines have been established that provide visual representations of position relative to the target, velocities, wind profiles, lift-to-drag ratio, ground speed, ground track, and distance to target.

The ballistic parachute described above is a tri-lobe canopy that has been designed to fall from a release point with minimum oscillation and rotation. In a no-wind situation, the canopy would fall straight to the ground from the initial release point. When placed in a force due to wind, the canopy moves with the force and position data is recorded. In that way, the relative strength of the wind force is measured and can be removed from the position data of the system under test.

The ballast under the tri-lobe canopy, shown in Figure 11, should be sufficient so that the canopy falls at the same rate as the system under test. An example wind profile is displayed in Figure 10. The wind vector has been broken out into north and east components. The magnitude of these components and the descent rate are given for reference. All velocities are shown with respect to altitude to give a perspective of what the system under test had to go through while falling to the ground.

Using this wind information, the wind-corrected position, velocities, and lift-to-drag ratio can be computed. As seen in Figure 12, the actual position of the decelerator system and the theoretical, 'no-wind' flight path differ. Since the ballistic parachute moved northeast from the initial drop spot, the flight path is corrected by stretching the original out toward the southwest. Position is calculated by decomposing wind data into north and east components, then subtracting the change in wind from the actual position.

If the ballistic and controlled units were released at the same moment, and the decent rates matched, the precise winds that the controlled system experienced would be characterized by the ballistic system. One indication that the wind data used for correction is valid is that the ground speed becomes constant through the descent as shown in Figure 13. The original ground velocity contains variations due to flying into and out of the wind. If wind speeds are nullified, no variation is seen.

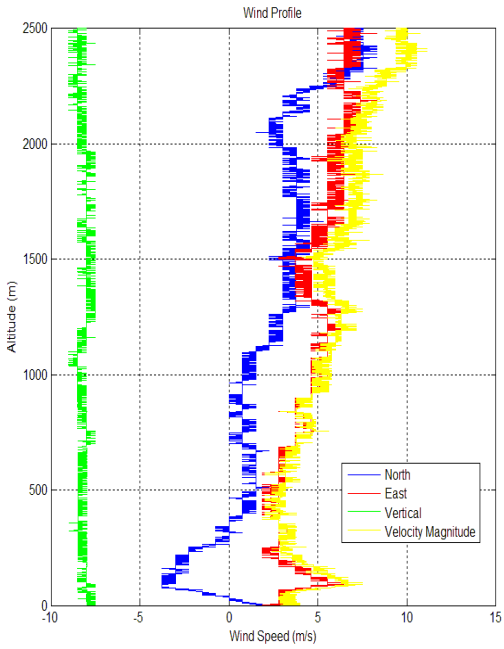

Figure 10. Wind Profile

Figure 11. Windpak System

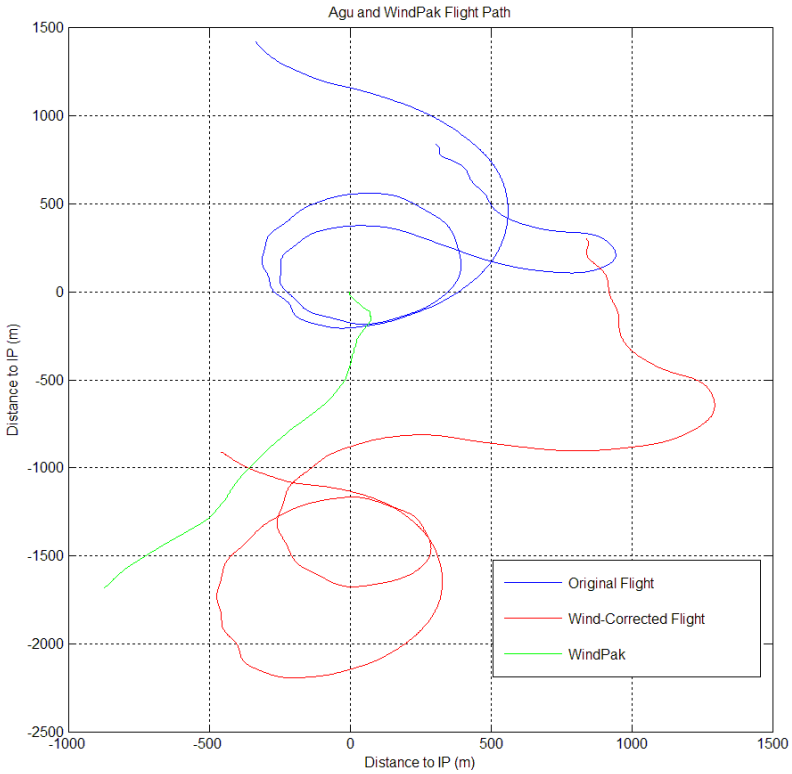

Figure 12. Original and Wind-Corrected Position.

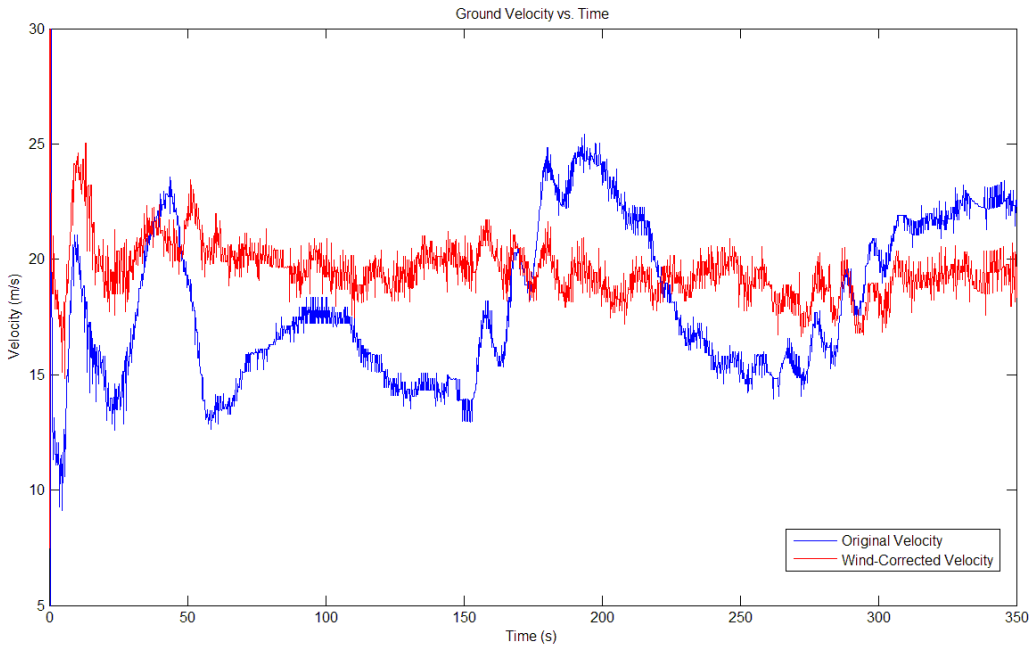

Figure 13. Original and Wind-Corrected Velocity.

V. Conclusions

The data presented above is a sample set of measured and calculated information that has become a part of the JPADS ACTD program. Both the sensor suite and the post-processing capabilities developed at Natick Soldier Center will continue to expand as the testing of decelerator systems carries on. Strain link and video data are desired to further characterize the systems under test.

VI. Acknowledgements

It has been an honor and pleasure working with the various men and women of the armed services throughout the testing process that produced this data. The authors would like to thank the US Army Natick Soldier Center Airdrop/Aerial Delivery Directorate, Yuma Proving Grounds, Joint Forces Command, and the Air Force Air Mobility Command for support and funding to produce the work presented above.

VII. References

[1]Manolakis, D., and Proakis, J., *Digital Signal Processing*, 3rd ed., Prentice Hall, Upper Saddle River, New Jersey, 1996, Chaps. 1, 8, 9.

[2]Oppenheim, A., and Schafer, R., *Discrete-Time Signal Processing*, 2nd ed., Prentice Hall, New York, 1999, Chap. 3.

[3]Papoulis, A., and Pillai, S. U., *Probability, Random Variables, and Stochastic Processes*, 4th ed., McGraw Hill, Upper Saddle River, Boston, 2002, Chaps. 5, 9.

[4]Goodman, D., and Yates, R., *Probability and Stochastic Processes*, 1st ed., Wiley, New York, 1998, Chaps. 3,7.